A New Control Strategy Based on Reference Values Changing for Enhancing LVRT Capability of DFIG in Wind Farm

Zahra Rafiee*, Mansour Rafiee* and Mohammadreza Aghamohammadi*‡

*Faculty of electrical engineering, Shahid Beheshti University, Velenjak, Shahid Shahriari Square, Daneshjou Boulevard, Shahid Chamran Highway, Tehran, Iran, Tel: +98 912 104 1201, Fax: +982177310425

(z.rafiee@sbu.ac.ir, m_rafiee@sbu.ac.ir, m_aghamohammadi@sbu.ac.ir)

‡ Corresponding Author; Mohammadreza Aghamohammadi, Shahid Beheshti University, Shahid Shahriari Square, Daneshjou Boulevard, Shahid Chamran Highway, Tehran, Iran, Tel: +98 912 104 1201, Fax: +982177310425, m_aghamohammadi@sbu.ac.ir

Received: 06.09.2019 Accepted:12.10.2019

Abstract- Low voltage ride through (LVRT) capability enables a doubly fed induction generator (DFIG) – based wind farm (WF) to remain online supporting the electric grid during fault condition. This paper proposes a control-based strategy for improving LVRT capability of DFIG, in which by changing active and reactive powers reference values following a voltage dip (VD) condition. Moreover, the direct power control (DPC) method is modified to adaptively change the reference values based on the severity of VD. In the proposed modified DPC (MDPC) method, the parameters of the PI controllers are tuned using the imperialist competitive algorithm (ICA). For activating/deactivating the proposed strategy, a voltage dip index (VDI) is proposed which is updated within a moving time window including samples measured by phasor measurement unit (PMU). In order to evaluate rout mean square (RMS) value of the voltage from the measured values by PMU, the DFT technique is used. For activating/deactivating the control strategy, two threshold values α and β are defined. In the active mode, the active and reactive power are changed to zero and one p.u, while in the deactivate mode theses are changed to one and zero p.u, respectively. Based on the proposed control strategy, during a VD condition, DFIG will be able to smooth the DC-link voltage fluctuations and significantly reduces the oscillations of the stator and rotor currents. The simulation results show the effectiveness of the proposed control strategy for improving LVRT capability of DFIG.

Keywords Doubly fed induction generator (DFIG); low voltage ride through (LVRT); direct power control (DPC); voltage dip, imperialist competitive algorithm.

NOMENCLATURE			
L_s	Stator inductance	ω_e	Synchronous angular speed
L_r	Rotor inductance	ω_r	Rotor angular speed
L_{lr}	Rotor leakage inductance	$\omega_s = \omega_e - \omega_r$	Relative speed of rotor respect to stator
L_{ls}	Stator leakage inductance	ω_{rm}	Mechanical rotor angular speed
L_m	Mutual inductance	p	Number of machine paired poles
R_s	Stator resistance	P_s ,Q_s	Stator active and reactive power
R_r	Rotor resistance	P_r ,Q_r	Active and reactive power rotor
i_s	Stator current vector	P ,Q	Active and reactive power generator
i_{sd} ,i_{sq}	d & q-axis stator current	T_m	Mechanical torque

i_{sd-ref} , i_{sq-ref}	d & q-axis stator current reference	σ	Coupling coefficient
i_r	Rotor current vector	τ_s	Stator time constant
i_{rd} , i_{rq}	d & q-axis rotor current	s	Slip
i_{rd-ref} , i_{rq-ref}	d & q-axis rotor current reference	EMF_r^r	Induced electrical motive force in the rotor in the rotor reference frame
i_r^s	Rotor current in the stator reference frame	EMF_r^s	Induced electrical motive force in the rotor in the stator reference frame
i_r^r	Rotor current in the rotor reference frame	U_s	Stator voltage magnitude
$i_{dqr-ref}$	dq-axis rotor current reference	P_2 & Q_2	Active and reactive power at the receiving bus.
i_{dqs}	dq-axis stator current	U_2 and U_1	Bus voltages
i_{gd} , i_{gq}	d & q-axis GSC current	φ	Power angle
u_{rd} , u_{rq}	d & q-axis rotor voltage	δ	Load angle
u_r^r	Rotor voltage in the rotor reference frame	I	line current
u_{gd} , u_{gq}	d & q-axis GSC voltage	R_{filter} , L_{filter}	Resistance and inductance filter
λ_{sd} , λ_{sq}	d & q-axis stator flux linkage	R_{Line} , L_{Line}	Resistance and inductance of transmission line
λ_{rd} , λ_{rq}	d & q-axis rotor flux linkage	U_{RMS}	RMS value of the measured stator terminal voltage
λ_s^s	Stator flux in the stator reference frame	λ_s^r	Stator flux in the rotor reference frame

1. Introduction

With the growing use of renewable energy, wind power has gained popularity as a source of electrical energy in many countries, such that the global wind power cumulative capacity reached 591 GW in 2018 [1]. Wind power plants like other power plants can affect voltage, frequency, stability and security of the network. DFIG-based wind turbines (DFIG-WT) are widely utilized for wind farms due to their capability for decoupled control of active and reactive powers, high efficiency, light weight and good speed control [2], [3]. However, DFIG-WT is vulnerable to low voltage conditions. The VD at the point of common coupling (PCC) of DFIG results DC-link over voltage and rotor over current at the beginning and end of the dip period [4]. These phenomenon can damage the electronic power devices of the DFIG and cause the WF to trip from the grid due to the lack of LVRT capability [5], [6]. However, tripping of WF is not a suitable strategy. Based on the LVRT requirements, WF must remain connected to the grid during a VD condition [7].

Generally, during a voltage dip, WFs are supposed to contribute to stability improvement and voltage recovery of the network by generating the reactive power. In addition, immediately after VD clearance, WFs must be able to provide active power for maintaining network stability. For enhancing the LVRT capability of the DFIG, various strategies have been proposed which can be classified in three categories: 1) device-based approaches, 2) control-based approaches, and 3) device and control-based approaches. A widely used device for LVRT is the crowbar resistor that is utilized in the rotor circuit causing the rotor side converter (RSC) to be blocked. This strategy is only used for protecting electronic devices during severe VD conditions. By connecting the crowbar resistor, DFIG is converted to squirrel cage induction generator (SCIG) which loses its controllability and absorbs more reactive power from the grid causing more decrease in the PCC voltage [8]. DC-chopper in parallel with the capacitor at the DC-link is another device for protecting DC-link against overvoltage. There are other device-based approaches trying to improve LVRT capability, namely stator dynamic composite fault current limiter in the stator [9], DC-chopper and series dynamic resistors for crowbar resistance [10], energy storage integration in DFIG-based WF [11], dynamic voltage restorer [12]–[15]. However, using device-based strategies need extra hardware devices resulting in cost increase and reliability reduction for DFIG. For these reasons, researchers often adopt control-based approaches to overcome the drawbacks of the device-based approaches.

In addition, control-based approaches for LVRT enhancement such as setting the electrical reference torque of DFIG to zero during VD condition [16], control of RSC by tracking the stator flux linkage [17], control of RSC by changing the rotor reference current [18], reverse current tracking in which the rotor current is controlled to track stator current reversely by a certain proportion [19], injecting additional feed-forward transient compensation terms into the outputs of the RSC current controller [20], instantaneous power feedback scheme [21], and fuzzy second order integral terminal sliding mode control which has been proposed and used for both RSC and grid side converter (GSC) [22] can only smooth rotor over current and DC-link over voltage oscillations without increasing the voltage at the PCC. For VD conditions, some of these approaches have not discussed the proper strategies for GSC and DC-link voltage in detail. For these reasons, some of the researchers have been proposed device and control based approaches [23].

In this paper, by changing reference values of active and reactive powers and without using any additional device, a new control-based approach is proposed for LVRT enhancement using a MDPC strategy. In this approach, during a VD condition, active and reactive powers reference values are changed. This method suppresses the rotor over current and decreases the DC-link voltage fluctuations and also increases the voltage at the PCC during a VD condition. For this purpose, a VDI calculated by received information from PMUs is proposed, by which reference values of powers can be changed properly. The parameters of the PI controllers of RSC and GSC in MDPC are optimized using the ICA in which the sum of the sample values in the discrete Fourier transform (SMVS-DFT) is used for evaluating the objective function. In addition to numerical simulation, an analytical analysis of the transient behaviour of the DFIG during VD condition is carried out. The proposed control approach is validated by using dynamic model of DFIG connected to the grid.

This paper is organized as follows. Section 2 presents the general overview of the proposed strategy. Section 3 discusses about the steady-state model of the DFIG. In Section 4, the transient behaviour of the DFIG is examined during VD event. Section 5 explains the principle of the proposed strategy. The proposed control strategy is introduced in Section 6 in detail. Then, simulation results are presented in Section 7. Finally, some conclusions are reached in Section 8.

2. General overview of the proposed strategy

In this paper, for improving LVRT capability of DFIG against VD conditions, a new technique of the control based strategy is proposed. The proposed control strategy works continuously within a moving time window in which voltage is measured by PMU from which VDI is evaluated for activating the control strategy. The length of the moving time window is 20 ms including 400 samples provided by PMU. The moving time window is updated continuously by one sample. In the proposed approach, following occurrence of a VD at the PCC, active and reactive power reference values are changed causing mitigation of rotor over current, decreasing DC-link voltage fluctuations and increasing voltage at the PCC. In this approach, a modified DPC is used for fast regulation of DFIG output powers. The proposed MDPC method is a hybrid mix of direct power and vector control methods. The DFIG connected to the electric network is equipped with six PI controllers, two controllers for RSC, three for GSC, and one for controlling rotor speed using pitch control. PI controllers' parameters are optimized with ICA in which PI parameters are tuned by changing active and reactive power reference values at the steady-state and transient behaviour. In order to evaluate the performance of the PI controllers, in steady state condition, by changing active and reactive power reference values using a look-up table, proper simulations of DFIG are carried out. Finally, in order to evaluate the ability of the proposed control approach for enhancing LVRT capability during a VD condition, the performance of the proposed control approach is examined for various VD percentages. All calculations and simulation studies are carried out by MATLAB/Simulink®.

3. DFIG Modelling

In this study, DFIG is modelled by the detailed dynamic model using the following voltage equations specified in the synchronous reference frame [24]:

$$\begin{cases} u_s = R_s i_s + d\lambda_s / dt + j\omega_e \lambda_s \\ u_r = R_r i_r + d\lambda_r / dt + j(\omega_e - \omega_r)\lambda_r \end{cases} \quad (1)$$

So, the flux equations can be shown as:

$$\begin{cases} d\lambda_s / dt = u_s - R_s i_s - j\omega_e \lambda_s \\ d\lambda_r / dt = u_r - R_r i_r - j(\omega_e - \omega_r)\lambda_r \end{cases} \quad (2)$$

In order to investigate the behaviour of the DFIG, the flux and current equations of the stator and the rotor have been expressed as:

$$\begin{cases} i_s = (L_r \lambda_s - L_m \lambda_r) / (L_s . L_r . \sigma_r) \\ i_r = (-L_m \lambda_s + L_s \lambda_r)(L_s . L_r . \sigma_r) \end{cases} \quad (3)$$

By substituting Eq. (36) and Eq. (37) into Eq. (35) the following state space equations can be derived:

$$\begin{cases} \dot{\lambda}_s = u_s - R_s \times (L_r \lambda_s - L_m \lambda_r) / (L_s . L_r . \sigma_r) - j\omega_e \lambda_s \\ \dot{\lambda}_r = u_r - \dfrac{R_r}{L_s . L_r . \sigma_r} \times (-L_m \lambda_s + L_s \lambda_r) - j(\omega_e - \omega_r)\lambda_r \end{cases} \quad (4)$$

4. The transient behaviours of the DFIG under VD condition

DFIG is highly sensitive to changes in its terminal voltage. Generally, when a disturbance occurs in the network causing a VD at the DFIG terminal, if the necessary actions are not taken, the following problems can arise:

- Stator flux fluctuations
- Increase in the electromotive force in the rotor winding
- Increase in the rotor current
- Increase in the DC link voltage
- Swing in torque and speed

When the voltage at the PCC decreases due to a symmetrical fault in the network, the induced electromotive force in the rotor reference frame EMF_r^r is expressed as [25]:

$$EMF_r^r = L_m / L_s . U_s [s(1-g) e^{j(\omega_e - \omega_r)t} - g . (\frac{1}{\tau_s} + j\omega_r) e^{-j\omega_r t} e^{-t/\tau_s} / j\omega_e] \quad (5)$$

where $\tau_s = L_s / R_s$ is the time constant of the stator winding and g refers to the VD percentage. By neglecting $1/\tau_s$, Eq. (5) can be simplified as:

$$EMF_r^r = L_m / L_s . U_s [s(1-g) e^{j(\omega_e - \omega_r)t} - g(1-s) e^{-j\omega_r t} e^{-t/\tau_s}] \quad (6)$$

From Eq. (6), it can be seen that at the initial moments of the fault (t = 0), the induced $EMF_r^r(0)$ is relatively large due to the DC offset in the flux. For example, for s = - 0.2 and g = 1, the value of the $EMF_r^r(0)$ becomes $1.2U_S L_m / L_S$ in the initial moments, which is 6 times the normal value.

5. Principle of the proposed method

In this section, the principle of the proposed control method for enhancing LVRT capability is explained. The enhancement of LVRT capability is based on the mitigation of rotor current and increase of PCC voltage, which are achieved by changing active and reactive power reference values

2.1. Control of the rotor current by active power reference value

Using vector control theory, the stator voltage vector u_s is orientated with the d-axis grid voltage as shown in Fig. 1, the dq-axis grid voltage will be as follows [26]–[28]:

$$u_{qs} = 0, \qquad u_{ds} = \sqrt{u_s^2 - u_{qs}^2} = u_s \tag{7}$$

So,

$$i_{ds} = (\lambda_s - L_m i_{dr}) / Ls \ , \ i_{qs} = -L_m i_{qr} / L_s \tag{8}$$

$$P_s = 3u_{qs} i_{qs} / 2 \ , \ Q_s = 3u_{qs} i_{ds} / 2 \tag{9}$$

Substituting Eq (8) into (9), the dq-axis rotor currents can be evaluated as follows:

$$\begin{cases} i_{dr} = -\left(\dfrac{2L_s}{3u_{ds}L_m}\right)P_s - \left(\dfrac{R_s}{\omega_e L_m}\right)i_{qs} \\ i_{qr} = \left(\dfrac{2L_s}{3u_{ds}L_m}\right)Q_s + \left(\dfrac{R_s}{\omega_e L_m}\right)i_{ds} - \left(\dfrac{1}{\omega_e L_m}\right)u_{ds} \end{cases} \tag{10}$$

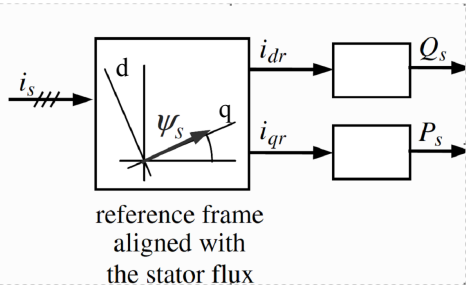

Fig 1. Vector control strategy [28].

By neglecting resistance of the stator winding in Eq. (9) and Eq. (24), the following can be obtained:

$$\begin{cases} i_{dr} = -2L_s P_s / (3u_{ds} L_m) \\ i_{qr} = 2L_s Q_s / (3u_{ds} L_m) - u_{ds} / (\omega_e L_m) \end{cases} \tag{11}$$

As it can be seen in Eq. (10) and Eq. (11), the behaviour of idr and iqr are decoupled and idr is directly proportional to Ps and iqr is directly related to Qs. Therefore, by changing the active and reactive power reference values, the dq-axis rotor currents can be controlled.

2.2. Control of the PCC voltage by reactive power reference value

Using two-bus system shown in Fig.2, the relationship between voltage U_2 and reactive power Q can be derived.

Using corresponding phasor diagram shown in Fig.3, the following equations can be obtained:

$$(U1 - U2)^2 = \Delta U^2 = \Delta U_R^2 + \Delta U_X^2 = (RI\cos\varphi + XI\sin\varphi)^2 + (XI\cos\varphi - RI\sin\varphi)^2 \tag{12}$$

Neglecting ΔU_X compared to ΔU_R, the VD can be obtained with respect to P_2 and Q_2:

$$\Delta U = RI\cos\varphi + XI\sin\varphi \tag{13}$$

$$\Delta U = \frac{RIU_2\cos\varphi + XIU_2\sin\varphi}{U_2} = \frac{RP_2 + XQ_2}{U_2} \tag{14}$$

where P_2 and Q_2 are active and reactive power R and X, U_2 and U_1 are voltage buses, and I is current line. Eq. (12) can be rewritten as follows:

$$U_2 = X\,(Q_2 + R\ /\ X\ .P_2) / \Delta U \tag{15}$$

Since R< X, the term $R\ /\ X\ .P_2$ is smaller than Q_2, so it can be concluded that the voltage is mainly dominated by the reactive power. Therefore, during a VD event for increasing the voltage of the PCC, it is sufficient to increase the reactive power reference value.

6. Proposed method

In the previous sections, it is shown that by changing active and reactive power of DFIG, it is possible to control rotor current and PCC voltage. According to this fact, in the proposed control strategy, during a VD event in order to reduce rotor current and increase PCC voltage, active and reactive powers of DFIG should be decreased and increased respectively. In Eq. (15), U_2 is calculated in terms of X, Q_2, and U_1. So, Q_2 is in terms of U_2, X, and U_1 ($Q_2 = U_2 \Delta U / X$).

Since the capacity of the majority of the DFIG-based WF unit is low and it is about 50 -100 MW special in Iran country [29] and the VD caused the blackout is big about 20% -0%, the DFIG must inject the maximum of its reactive power during VD conditions. Therefore, the active power must decrease to zero.

These changes support network voltage and avoid rotor over current. Figure 4 shows the decision algorithm for activating and deactivating the control strategy when a VD occurs. At each time instant, the measured VRMS is compared with the voltage reference value (1p.u) from which VDI is calculated. According to the decision algorithm shown in Figure 8, for VDI(t) $\geq \alpha$, active and reactive power reference

values are set to 0 and 1 respectively. Once VDI(t) gets smaller than β, the reference values are returned to the normal setting.

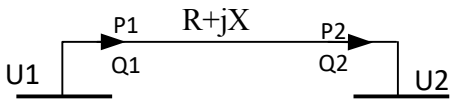

Fig 2. Two-bus system

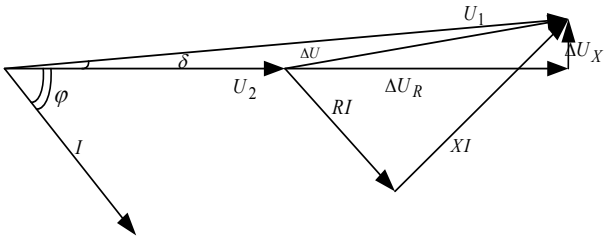

Fig 3. Voltage phasor diagram

In this paper, based on the changing active and reactive power reference values and using MDPC, a new control strategy is proposed to increase the PCC voltage and suppress the DC-link voltage and rotor current resulting in LVRT capability enhancement. The key issue in the proposed control method is to increase the PCC voltage using a control-based approach during a VD event. MDPC is used for fast regulation of DFIG output powers. The proposed MDPC is a hybrid mix of direct power [30] and vector control methods, in which based on the vector control theory, the generator terminal voltage aligns with the d-axis of the synchronous reference frame. Figure 4 shows the structure of the proposed control strategy. As it can be seen, the on-off hysteresis controllers of DPC are replaced with PI controllers. Similar to the DPC strategy, the input signals of the PI controllers are the stator output powers error vectors, used to build rotor voltage. The built rotor voltage is given to pulse width modulation unit (PWM) to create switching signals for RSC. By the proposed approach, following a VD, the following capabilities for LVRT of DFIG could be provided:

- Ensuring that DFIG can stay connected to the grid during a VD event by effectively decreasing the stator and rotor currents as well as reducing the DC-link voltage.
- Contributing to network voltage support by providing a reactive power in response to a VD at the PCC depending on the VD level of the PCC (e.g. 4% reactive power for 1% VD [16]).
- Participating in the network frequency control by generating sufficient active power after the fault clearance (e.g. larger or equal to 95% of the pre-fault active power in 100 ms after fault clearance [31]).

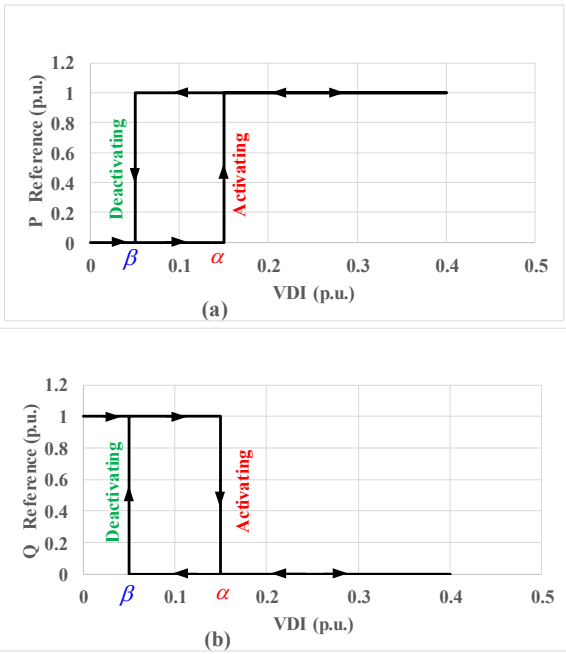

Fig 4. Decision algorithm for changing active and reactive power references: (a) reactive power, (b) active power.

In order to apply the proposed control strategy, first, it is necessary to tune PI controllers' parameters of DFIG as shown in Fig. 5. For this purpose, DFIG is modelled in the state space with six-controlled current sources and by using ICA optimization algorithm [32]–[34], the PI control parameters are tuned optimally. The ICA and SMVS-DFT as objective function [33]–[35]. is utilized to design PI controllers to control steady-state and transient behaviour of DFIG. Then, by setting optimal PI controllers' parameters for DFIG (by tracking active and reactive power reference values) its steady state condition is evaluated.

The proposed control approach is continuously performed within a moving time window with the length of 20 ms including 400 samples which are gathered by a sampling rate of 20 kHz using PMU. It is worth noting that the moving window is updated for each sample (50 μs). Figure 5 shows the real time process of the proposed control strategy consisting of the following steps:

Step 1- At each moving time window for 400 samples provided by PMU by using discrete Fourier transform (DFT) the RMS value of the voltage magnitude at the terminal of DFIG is obtained.

Step 2- Using measured URMS, the VD index (VDI) is evaluated for activating/deactivating the proposed control strategy.

$$VDI(t) = 1.0 - U_{RMS}(t) \tag{16}$$

Step 3- The VD index (VDI) is compared to the threshold value α for activating the proposed control strategy.

$$If \;\; VDI(t) > \alpha \;\rightarrow Active\;\; Control \;\; Strategy$$

Step 4- The VDI(t) is compared to the threshold value β for deactivating the proposed control strategy

$$If \quad VDI(t) < \beta \rightarrow Deactive\ Control\ \ Strategy$$

As long as the VDI(t) remains between two threshold values $(\alpha > VDI(t) > \beta)$ the control strategy remains active. Figure 6 shows the decision flow for activating/deactivating the proposed control strategy. It is worth noting that choosing proper values for α and β depend on the sensitivity of the voltage magnitude to reactive power compensation which is related to the short circuit capacity of the terminal of DFIG.

7. Simulation results

In order to demonstrate the effectiveness of the proposed control strategy, it is applied on a DFIG connected to the main grid through a transmission line as shown in Fig. 7.

2.3. Optimization of the PI controllers' parameters

The parameters of the PI controllers are tuned by the ICA, using the following objective function (SMVS-DFT):

$$OF = 25\Delta U_{DC} + 10\Delta P_s + 10\Delta Q_s + 8\Delta\omega_r + 30\Delta i_{dr} + 30\Delta i_{qr} \quad (17)$$

The weighting coefficients of the variables consisting OF have been selected based on the empirical analysis of the variables behaviour with respect to their reference values. The optimized parameters are given in Table 1.

Table 1. Parameters of PI controllers.

Element	*Variable control*	*KP*	*KI*
RSC	*Active power*	*0.1*	*10*
	Reactive power	*0.1*	*10*
GSC	*DC-link voltage*	*0.01*	*0.01*
		100	*0.01*
	Reactive power	*99.155*	*77.776*
Rotor	*speed*	*50*	*1*

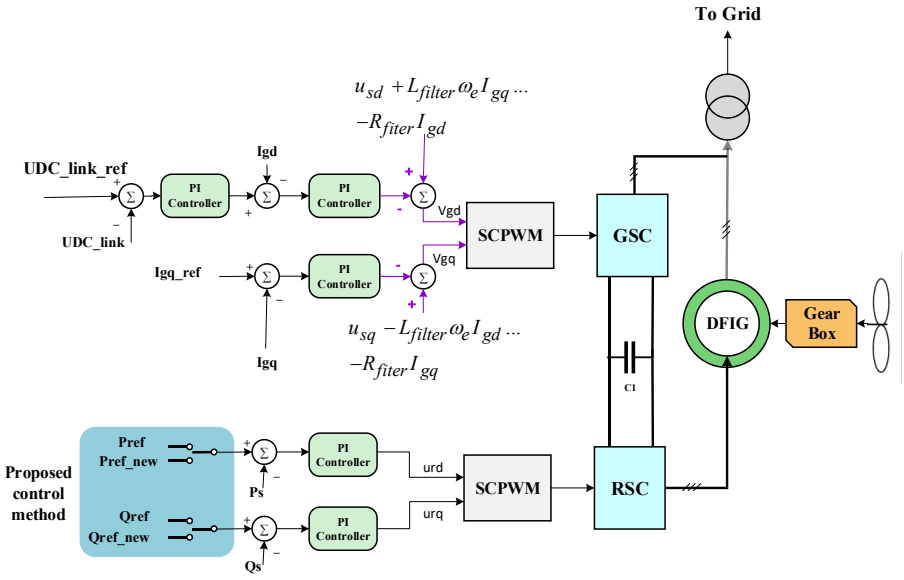

Fig 5. The proposed control strategy consisting of decision algorithm and MDPC.

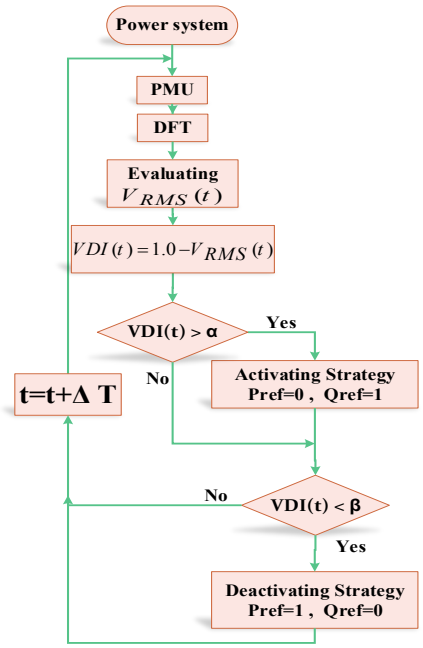

Fig 6. The real time process of the proposed control strategy.

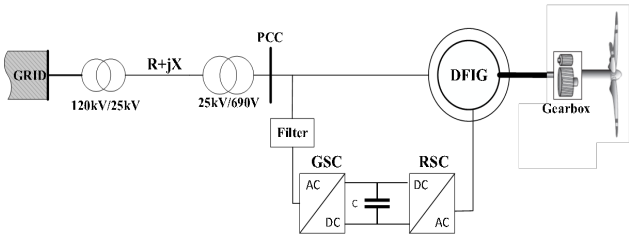

Fig 7. System under study.

The weighting coefficients of the variables consisting OF have been selected based on the empirical analysis of the variables behaviour with respect to their reference values. The optimized parameters are given in Table 1.

2.4. Transient behaviour of DFIG during VD conditions

In order to peruse transient behaviour of the DFIG during a VD condition, the following assumptions are considered:

A. DFIG operates in super-synchronous speed with the potential for generating maximum rotor over current.

B. Wind speed variation is negligible, due to short duration of fault,

C. DFIG is operating at the steady state before VD condition.

In order to validate the effectiveness of the proposed control strategy for both steady state behaviour of DFIG and LVRT capability during transient behaviour of DFIG, five scenarios have been simulated and analyzed. Also, switching frequency and sampling time in PWM are considered 1 kHz and 50 μs, respectively.

Scenario 1-Tracking the active power reference:

In this scenario, the performance of the proposed control strategy for active power tracking in a normal condition is studied. The active power reference was stepped according to the vector [0.8 , 0.6 , 0.2 , .8 , 1] p.u at time vector [0, 1, 2 , 3 , 4] s, while the reactive power is kept constant at 0.065 p.u.. Figure 8 shows the simulation results. As it can be seen, the active power has tracked the active power reference vector quickly with a small overshoot. The d-axis stator current has changed proportional to the active power reference vector. Rotor speed has absorbed the additional kinetic energy during change of active power reference which has caused a reverse change in the rotor speed

Scenario 2-Tracking the reactive power

In this scenario, the performance of the proposed control strategy for reactive power tracking in a normal condition is studied. The reactive power reference was stepped by the vector [0, 1 , 0.5 , 0 , 0.6] p.u at time vector [0 , 1 , 2 , 3 , 4] s, while at each step, the corresponding active power reference is calculated using $\sqrt{1-Q^2}$ as upper limit ($P \le \sqrt{1-Q^2}$). Figure 9 shows the simulation results. As it can be seen, the reactive power has tracked the reactive power reference vector very well and quickly with a small overshoot. The q-axis stator current has changed proportional to the reference reactive power vector. The DFIG terminal voltage has changed proportional to the reactive power which causes the increase of generator terminal voltage.

In the next three scenarios, the LVRT capability of DFIG during transient period following a three-phase fault at t=3s with duration of 300ms in the network which causes different VD conditions for DFIG is investigated. Decision block detects the fault after 20ms because discrete Fourier transform is used for phasor measurement. The rotor current limit is 2p.u and DC-link voltage limit is 1.2p.u of rated value [36].

Scenario 3- Transient behavior of DFIG for 20% VD

Figure 10 shows the results of the simulation for the 20% VD in the network. It is worth noting that each figure includes 6 sub-figures which have two identical variables. Because of the shortage of space for sub-figures, the legend, which is identical for all sub-figures, is placed on the upper right corner of only one sub-figure as reprehensive for all sub-figures. In this set of results, the reactive and active powers injected into the network, the rotor speed, the stator current components in the synchronous reference frame, the DC link voltage, and finally the voltage at generator terminal are shown. As it can be seen, reactive and active powers are well suited at the normal conditions to their reference values. When the VD occurs at the generator terminals, the values of the active and reactive power reference values are immediately changed based on the decision strategy after detection of the VD. As a result, active and reactive powers are greatly decreased and increased respectively and stator currents (i_{dq}) are also well changed. Due to injection of 2.5 MVAR reactive power to the grid, the terminal voltage is increased by about 0.1 p.u. Also, due to the reduction of active power generation, the stator and rotor currents during the fault are decreased compared to the condition that the power reference has not changed. As it can

be seen in Fig. 10e for 20% VD, the DC link voltage fluctuation is low.

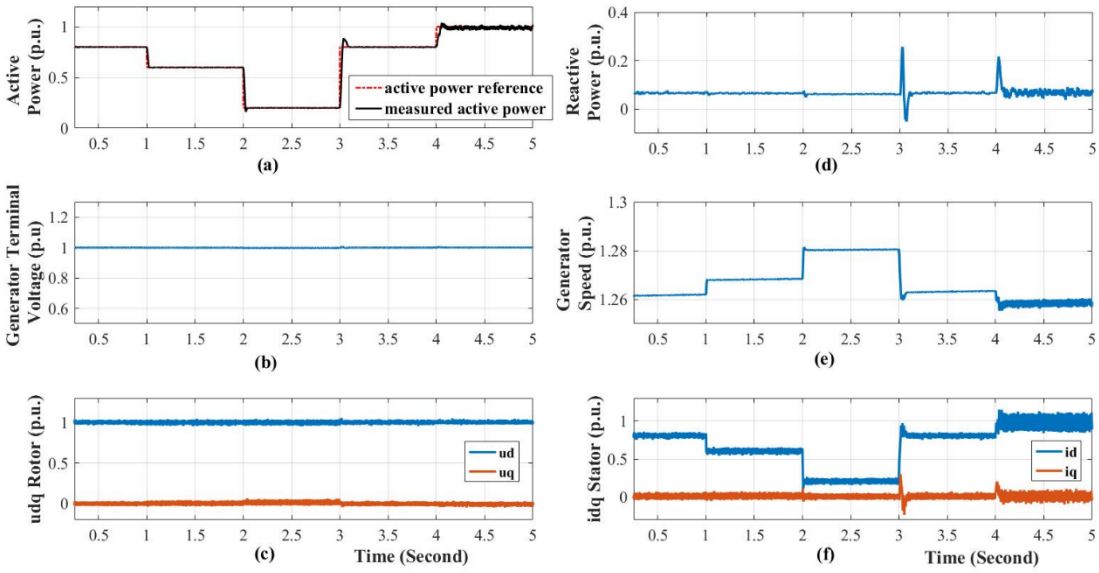

Fig 8. Variation of DFIG variables during tracking of active power reference: (a) Active power, (b) Generator terminal voltage, (c) udq rotor, (d) Reactive power, (e) Generator speed, (f) idq stator.

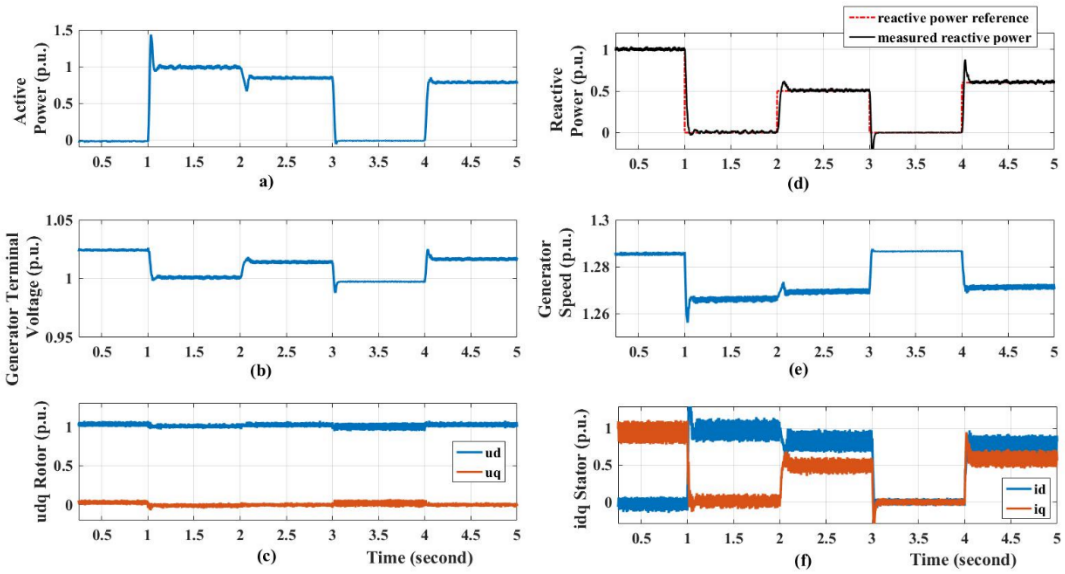

Fig 9. Variation of DFIG variables during tracking of reactive power reference: (a) Active power, (b) Generator terminal voltage, (c) udq rotor, (d) Reactive power, (e) Generator speed, (f) idq stator.

Scenario 4- Transient behavior of DFIG for 40% VD

Figure 11 shows the results of the simulation for the 40% VD in the network. Comparing to scenario 3, no significant difference can be seen in the results and this is because the amount of VD is not much severe. The improvement in terminal voltage is the same as in scenario 3. The generator terminal voltage increased about 0.1p.u, which is proportional to the network's short circuit level and reactive power injection into the network. DC-link voltage fluctuation is low.

Scenario 5- Transient behavior of DFIG for 60% VD

Figure 12 shows the results of the simulation for the 60% VD in the network. Comparing to the previous scenarios, the improvement achieved by the proposed control strategy is significant. DC-link voltage which is increased up to 1600 V is reduced to 1300 V. Increase in the terminal voltage is the same as the previous scenarios. Also, the stator currents are relatively improved.

Figure 13a) comparatively shows the rotor speed for three scenarios in which following a decrease in active power, rotor speed is increased within its limit by relatively equal amount for three scenarios.

Figure 13b shows the rotor current variation for three scenarios in which for the case of 60% VD the current is increased more than 2 p.u. which is controlled by the proposed approach.

It is worth noting that in the previous control-based methods [37]–[41] only the rotor current and DC link voltage have been improved for enhancing LVRT capability however and the PCC voltage has not been considered for improvement. In this paper, in addition to controlling rotor and stator currents and DC link voltage, the proposed method considers the behavior of PCC voltage and improve it. Comparing the previous works, since all efforts of the controller is employed for rotor and stator currents and DC link voltage, the their performance for these variables is better than the proposed method while their performance for PCC voltage is poor.

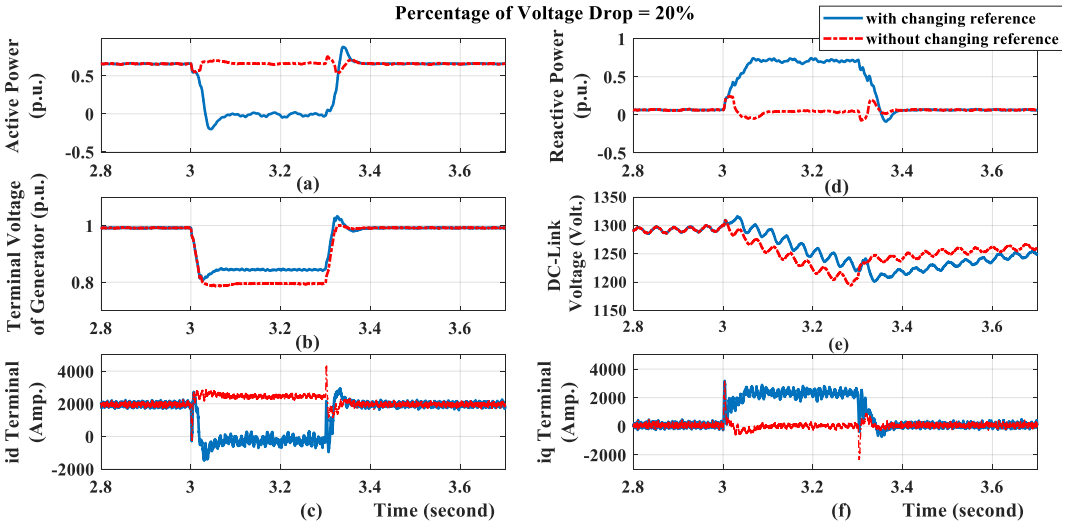

Fig 10. The simulation results for a three-phase fault in the network causing 20% VD.

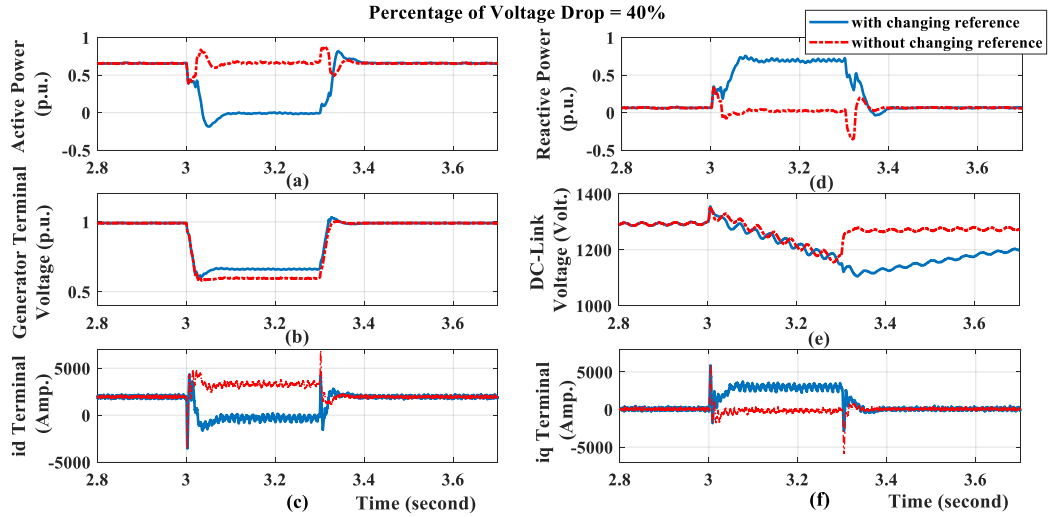

Fig 11. The simulation results for a three-phase fault in the network casuing 40% VD.

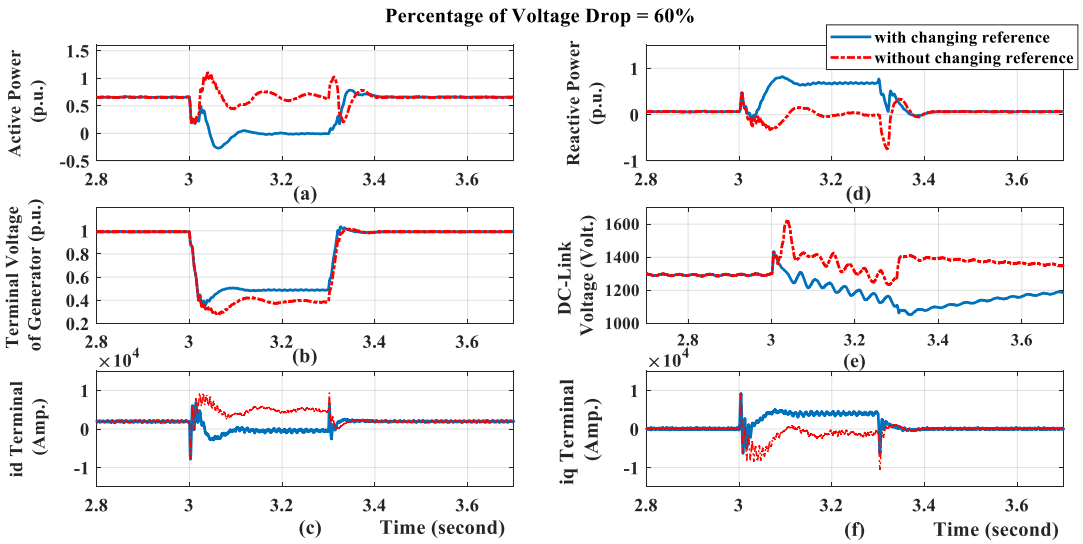

Fig 12. The simulation results for a three-phase fault in the network causing 60% VD.

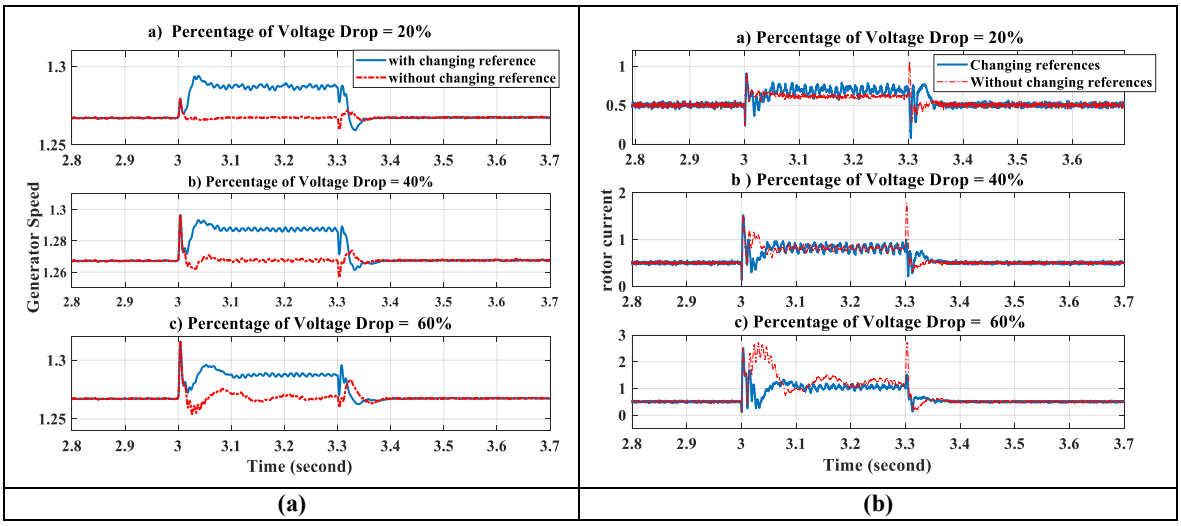

Fig 13. (a) The rotor speed for three types of VD event, (b) the rotor current (RMS values) for three types of VD event.

8. Conclusion

In this paper, for mitigating the side effects of a severe VD condition and improving LVRT capability of DFIG, a new control-based strategy is proposed in which by changing active and reactive power reference values, DC-link over voltage, rotor over current and terminal voltage can be properly controlled. In the proposed control strategy, the VDI is proposed as a detection index for activating and deactivating the proposed control strategy. In this approach, by using vector control theory, the direct power control method is modified to adaptively change the reference values based on the severity of VD while avoiding rotor current increase. In the proposed MDPC method, the parameters of the PI controllers are tuned using the ICA. The main advantage of the proposed control method is its control-based nature which makes it easy for implementation into the network without need for any additional devices. The simulation results show that for a severe VD condition, the proposed control strategy is able to decrease DC-link voltage and rotor current while increasing terminal voltage. The voltage improvement depends on the fault level of the terminal point and the amount of reactive power which can be injected into the grid by DFIG. For the case of 60% VD condition, the improvement in DC-link voltage and rotor current are relatively good which demonstrates the ability of the proposed control strategy for improving LVRT capability.

Appendix

Table A1. Induction machine parameters.

Rated power DFIG	2.5 MW	**Rotor voltage**	1975
Stator voltage	690 V	**Rotor rated current**	731 A
Stator rated current	2092 A	**Rotor leakage inductance**	0.1 p.u.
Magnetization inductance generator	5 p.u.	**Rotor resistance**	0.02 p.u.
Stator leakage inductance	0.1p.u.	**Number of pair of poles**	3

Stator resistance	0.01p.u.	Conversion ratio from stator to rotor	690/1975

Table A2. Line and grid parameters.

Grid	High voltage transformer	Line	Medium voltage transformer
S = 500MVA V_n = 120kV R_{mu} = 0.1 p.u. X_{mu} = 1.0 p.u.	P_n = 47 MW V_{n1}=120kV, R1=0.08/30 p.u., X_1 = 0.08 p.u. V_{n2}=25kV, R_2 = 0.08/30 p.u., X_2 = 0.08 p.u.	R_{Line} = 0.1153 ohm/km. X_{Line}= 1.05e-3 ohm/km. Line length = 10 km.	P_n = 3 MW V_{n1} = 25kV, R_1 = 0.025/30 p.u., X_1 = 0.025 p.u., V_{n2}= 690 V, R_2 = 0.025/30 p.u., X_2 = 0.025 p.u..

References

[1] "Global Wind Report 2018 | Global Wind Energy Council." [Online]. Available: https://gwec.net/global-wind-report-2018/. [Accessed: 09-Oct-2019].

[2] T. Douadi, Y. Harbouche, R. Abdessemed, and I. Bakhti, "Improvement Performances of Active and Reactive Power Control Applied to DFIG for Variable Speed Wind Turbine Using Sliding Mode Control and FOC," *Int. J. Eng. - Trans. A Basics*, vol. 31, no. 10, pp. 1689–1697, 2018.

[3] D. Icaza, F. Cordova, and F. Toledo, "System of Electrical Generation by Wind and Solar Sources in the Archaeological Surroundings of the Hill Curiquinga of Quingeo- Ecuador," in *2018 International Conference on Smart Grid (icSmartGrid)*, 2018, pp. 164–170.

[4] W. Teng and Y. Meng, "Rotor-reference-current-oriented control strategy for low-voltage ride-through of DFIG," *IEEJ Trans. Electr. Electron. Eng.*, vol. 13, no. 10, pp. 1421–1429, Oct. 2018.

[5] H. Shahbabaei Kartijkolaie, M. Radmehr, and M. Firouzi, "LVRT capability enhancement of DFIG-based wind farms by using capacitive DC reactor-type fault current limiter," *Int. J. Electr. Power Energy Syst.*, vol. 102, pp. 287–295, Nov. 2018.

[6] A. Hussein and A. Castellazzi, "Comprehensive design optimization of a wind power converter using SiC technology," in *2018 International Conference on Smart Grid (icSmartGrid)*, 2018, pp. 34–38.

[7] E. Jamila and S. Abdelmjid, "Comparative Study of the Performance of Static Synchronous Compensator, Series Compensator and Compensator /Battery Integrated to a Fixed Wind Turbine (RESEARCH NOTE)," *Int. J. Eng. - Trans. A Basics*, vol. 29, no. 4, pp. 581–589, 2016.

[8] M. Rahimi and A. Azizi, "Transient behavior representation, contribution to fault current assessment, and transient response improvement in DFIG-based wind turbines assisted with crowbar hardware," *Int. Trans. Electr. Energy Syst.*, vol. 29, no. 1, p. e2698, Jan. 2019.

[9] P. K. Gayen, D. Chatterjee, and S. K. Goswami, "An improved low-voltage ride-through performance of DFIG based wind plant using stator dynamic composite fault current limiter," *ISA Trans.*, vol. 62, pp. 333–348, May 2016.

[10] A. El Makrini, Y. El Karkri, Y. Boukhriss, H. Elmarkhi, and H. El Mossaoui, "LVRT Control Strategy of DFIG Based Wind Turbines Combined the Active and Passive Protections," *Int. J. Renew. Energy Res.*, vol. 7, no. 3, pp. 1258–1269, Sep. 2017.

[11] P. Tourou, J. Chhor, K. Gunther, and C. Sourkounis, "Energy storage integration in DFIG-based wind energy conversion systems for improved fault ride-through capability," in *2017 IEEE 6th International Conference on Renewable Energy Research and Applications (ICRERA)*, 2017, pp. 374–377.

[12] A. D. Falehi and M. Rafiee, "Enhancement of DFIG-Wind Turbine's LVRT capability using novel DVR based Odd-nary Cascaded Asymmetric Multi-Level Inverter," *Eng. Sci. Technol. an Int. J.*, vol. 20, no. 3, pp. 805–824, Jun. 2017.

[13] A. Darvish Falehi and M. Rafiee, "Fault ride-through capability enhancement of DFIG-based wind turbine using novel dynamic voltage restorer based on two switches boost converter coupled with quinary multi-level inverter," *Energy Syst.*, vol. 9, no. 4, pp. 1071–1094, Sep. 2017.

[14] S. Deepa and S. Rajapandian, "Harmonic Reduction Technique Using Flying Capacitor Based Z Source Inverter for a DVR," *Int. J. Eng. - Trans. C Asp.*, vol. 26, no. 3, pp. 309–314, Nov. 2012.

[15] E. El Hawatt, M. S. Hamad, K. H. Ahmed, and I. F. El Arabawy, "Low voltage ride-through capability enhancement of a DFIG wind turbine using a dynamic voltage restorer with Adaptive Fuzzy PI controller," in *2013 International Conference on Renewable Energy Research and Applications (ICRERA)*, 2013, pp. 1234–1239.

[16] L. Yang, Z. Xu, J. Ostergaard, Z. Y. Dong, and K. P. Wong, "Advanced Control Strategy of DFIG Wind Turbines for Power System Fault Ride Through," *IEEE Trans. Power Syst.*, vol. 27, no. 2, pp. 713–722, May 2012.

[17] D. Xiang, L. Ran, P. J. Tavner, and S. Yang, "Control of a Doubly Fed Induction Generator in a Wind Turbine During Grid Fault Ride-Through," *IEEE Trans. Energy Convers.*, vol. 21, no. 3, pp. 652–662, Sep. 2006.

[18] Z. Su, P. Wang, L. Tan, and P. Song, "An improved LVRT control method of MW level DFIG-based WECS," in *2014 17th International Conference on Electrical Machines and Systems (ICEMS)*, 2014, pp. 1400–1405.

[19] Huang Qingjun, Sun Mucun, Zou Xudong, Tong Li, Xiong Wei, and Chen Jianqing, "A reverse current tracking based LVRT strategy for doubly fed induction generator (DFIG)," in *IECON 2013 - 39th Annual Conference of the IEEE Industrial Electronics Society*,

2013, pp. 7295–7300.

[20] J. Liang, W. Qiao, and R. Harley, "Feed-forward transient current control for low-voltage ride-through enhancement of DFIG wind turbines," in *2011 IEEE/PES Power Systems Conference and Exposition*, 2011, pp. 1–1.

[21] Jun Yao, Hui Li, Yong Liao, and Zhe Chen, "An Improved Control Strategy of Limiting the DC-Link Voltage Fluctuation for a Doubly Fed Induction Wind Generator," *IEEE Trans. Power Electron.*, vol. 23, no. 3, pp. 1205–1213, May 2008.

[22] M. J. Morshed and A. Fekih, "A new fault ride-through control for DFIG-based wind energy systems," *Electr. Power Syst. Res.*, vol. 146, pp. 258–269, May 2017.

[23] M. Rahimi and M. Parniani, "Low voltage ride-through capability improvement of DFIG-based wind turbines under unbalanced voltage dips," *Int. J. Electr. Power Energy Syst.*, vol. 60, pp. 82–95, Sep. 2014.

[24] N. Z. Frede Blaabjerg, Dehong Xu , Wenjie Chen, "Dynamic Model of DFIG Under Grid Faults," in *Advanced Control of Doubly Fed Induction Generator for Wind Power Systems*, Hoboken, NJ, USA: John Wiley & Sons, Inc., 2018, pp. 297–340.

[25] S. Xiao, G. Yang, H. Zhou, and H. Geng, "An LVRT Control Strategy Based on Flux Linkage Tracking for DFIG-Based WECS," *IEEE Trans. Ind. Electron.*, vol. 60, no. 7, pp. 2820–2832, Jul. 2013.

[26] H. BENBOUHENNI, "Direct power control of a DFIG fed by a seven-level inverter using SVM strategy," *Int. J. Smart Grid - ijSmartGrid*, vol. 3, no. 2, pp. 54–62, Jun. 2019.

[27] H. habib0264 BENBOUHENNI, Z. Boudjema, and A. Belaidi, "Using Three-Level Fuzzy Space Vector Modulation Method to Improve Indirect Vector Control Strategy of a DFIG Based Wind Energy Conversion Systems," *Int. J. Smart Grid - ijSmartGrid*, vol. 2, no. 3, pp. 155–171, Nov. 2018.

[28] G. Abad, *Doubly fed induction machine : modeling and control for wind energy generation applications*. Wiley-Blackwell Pub, 2011.

[29] "Iran's largest wind farm commissioned | Windpower Monthly." [Online]. Available: https://www.windpowermonthly.com/article/1491599/irans-largest-wind-farm-commissioned. [Accessed: 10-Oct-2019].

[30] H. habib0264 BENBOUHENNI, "Comparative Study Between Direct Vector Control and Fuzzy Sliding Mode Controller in Three-Level Space Vector Modulation Inverter of Reactive and Active Power Command of DFIG-Based Wind Turbine Systems," *Int. J. Smart Grid - ijSmartGrid*, vol. 2, no. 4, pp. 188–196, Dec. 2018.

[31] J. J. Justo, F. Mwasilu, and J.-W. Jung, "Enhanced crowbarless FRT strategy for DFIG based wind turbines under three-phase voltage dip," *Electr. Power Syst. Res.*, vol. 142, pp. 215–226, Jan. 2017.

[32] E. Atashpaz-Gargari and C. Lucas, "Imperialist competitive algorithm: An algorithm for optimization inspired by imperialistic competition," in *2007 IEEE Congress on Evolutionary Computation*, 2007, pp. 4661–4667.

[33] Z. Rafiee, S. Ganjefar, and A. Fattahi, "A new PSS tuning technique using ICA and PSO methods with the fourier transform," in *Proceedings - 2010 18th Iranian Conference on Electrical Engineering, ICEE 2010*, 2010.

[34] Z. Rafiee, A. F. Meyabadi, and H. Heydari, "PSS parameters values finding using SMVSDFT objective function and a new technique for multi-objective function in a multi-machine power system," *Int. J. Power Energy Convers.*, vol. 6, no. 3, p. 252, 2015.

[35] Z. Rafiee and A. F. Meyabadi, "Optimal design of power system stabiliser using a new cost function and PSO algorithm," *Int. J. Power Energy Convers.*, vol. 3, no. 3/4, p. 253, 2012.

[36] A. H. Kasem, E. F. El-Saadany, H. H. El-Tamaly, and M. A. A. Wahab, "An improved fault ride-through strategy for doubly fed induction generator-based wind turbines," *IET Renew. Power Gener.*, vol. 2, no. 4, pp. 201–214, Dec. 2008.

[37] A. R. A. Institution of Engineering and Technology., P. Kaliannan, U. Subramaniam, and M. S. El Moursi, *IET renewable power generation.*, vol. 12, no. 15. Institution of Engineering and Technology, 2007.

[38] D. Xiang, L. Ran, P. J. Tavner, and S. Yang, "Control of a Doubly Fed Induction Generator in a Wind Turbine During Grid Fault Ride-Through," *IEEE Trans. Energy Convers.*, vol. 21, no. 3, pp. 652–662, Sep. 2006.

[39] H. Mahvash and S. A. Taher, "A look-up table based approach for fault ride-through capability enhancement of a grid connected DFIG wind turbine," *Sustain. Energy, Grids Networks*, vol. 10, pp. 128–140, Jun. 2017.

[40] S. A. A. Shahriari, M. Mohammadi, and M. Raoofat, "A new method based on state-estimation technique to enhance low-voltage ride-through capability of doubly-fed induction generator wind turbines," *Int. J. Electr. Power Energy Syst.*, vol. 95, pp. 118–127, Feb. 2018.

[41] C. J. Madan and N. Kumar, "Fuzzy grey wolf optimization for controlled low-voltage ride-through conditions in grid-connected wind turbine with doubly fed induction generator," *Simulation*, vol. 95, no. 4, pp. 327–338, Apr. 2019.